The effect of a temperature gradient on the phase formation inside a magnesia-chromite refractory in contact with a non-ferrous PbO-SiO_2-MgO slag

L. Scheunis[1*], A. Fallah-Mehrjardi[2], M. Campforts[3], P.T. Jones[1], B. Blanpain[1], A. Malfliet[1] and E. Jak[2]

[1] *Department of Materials Engineering, KU Leuven, Kasteelpark Arenberg 44, Box 2450, 3001 Heverlee, Belgium*

[2] *Pyrometallurgy Research Centre, School of Engineering, The University of Queensland, Brisbane, Queensland, Australia*

[3] *Research & Development, Umicore, Kasteelstraat 7, 2250 Olen, Belgium*

Abstract

Furnace relinings represent a major operating cost in pyrometallurgy. External cooling is, therefore, often used to reduce the chemical wear by limiting the slag infiltration depth, reducing the reaction kinetics and lowering the solubility of refractory components into the liquid slag. In this paper a new experimental setup is used to study the reaction between a synthetic PbO-SiO_2 based slag and a magnesia-chromite refractory under a temperature gradient. Forsterite (Mg_2SiO_4) is formed throughout the sample, removing SiO_2 from the infiltrated liquid slag. The resulting change in slag composition causes the liquidus temperature and the viscosity of the liquid to decrease, partially countering the effect of the applied temperature gradient and resulting in the complete infiltration of the sample. The extent to which external cooling prolongs the lifetime of an industrial furnace thus depends on the slag properties and how they are modified after reaction with the refractory.

Keywords

Refractory wear; PbO slag; temperature gradient; forsterite formation; slag infiltration

1 Introduction

Ceramic magnesia-chromite refractory bricks are commonly used in non-ferrous smelting furnace linings because of their high melting point, good mechanical properties at elevated temperatures and their ability to withstand aggressive conditions [1, 2]. Despite these properties, wear still occurs, eventually requiring a costly replacement of the lining. Reducing the wear increases the time between replacements, leading to a more efficient operation. Refractory wear is caused by a combination of chemical, thermal and mechanical stresses, with the chemical attack by liquid slag often being the most critical. The identification of the main degradation mechanisms in industrial environments is typically done using post mortem analyses [3, 4]; samples are taken from the lining after the final cooling of the reactor and the microstructure of these samples is analyzed and compared with the microstructure of the original bricks, thereby identifying the degradation mechanisms.

[*] Corresponding author: *tel:* +32-16-321780; *fax:* +32-16-321991
Email address: lennart.scheunis@mtm.kuleuven.be (L. Scheunis).

Chemical degradation is also studied using lab scale experiments under controlled conditions [5, 6], making it possible to better link the effect of a single parameter to the occurring wear mechanism. In order to perform these experiments several simplifications are made with respect to the industrial process: a single (often simplified) slag composition is used; the turbulence of the bath is in most cases not taken into account; the pO_2 is assumed to remain constant and, finally, most experiments are performed at constant temperature, typically the working temperature of the furnace. In reality, however, all industrial refractory linings have a temperature gradient between the hot face (i.e. the side in contact with the liquid bath) and the cold face (i.e. the side in contact with the shell of the steel vessel). Some furnaces even apply additional cooling of the lining by using water cooled copper plates at the cold face side in order to solidify the infiltrating slag and limit the reaction surface between slag and the porous refractory lining. The assumption of an isothermal system is, therefore, only valid when the slag does not deeply infiltrate the lining and the temperature in the infiltrated part of the refractory is thus close to the operating temperature of the furnace.

In order to investigate the effect of a temperature gradient on an infiltrated refractory sample a new setup is developed, based on an experimental setup typically used for freeze lining experiments [7-11] consisting of a water or air cooled probe, where the flow rate can be used to control the temperature at the probe side. In this paper a refractory sample is placed between the cooling probe and the liquid slag bath, thereby creating a temperature gradient over the refractory sample. This approach differs from the experimental setup currently used by Kaneko et al. [12-14] where a refractory sample is partially put in the hot zone of a furnace while the bottom of the refractory is kept in a colder part of the furnace resulting in a temperature gradient over the sample. A hole is drilled in the part of the sample in the hot zone and filled with slag. The main differences between that setup and the one used in this work are the ability of the latter to quench the samples after the experiment, the large slag volume in contact with the refractory sample and the ability to control the cold face temperature (and thus also the gradient) by the gas flow.

This new setup is used to investigate the effect of a temperature gradient on the infiltration behavior and the phase formation inside a porous magnesia-chromite refractory sample in contact with a synthetic PbO-SiO_2-MgO slag. PbO systems are known to deeply infiltrate the sample [15] and previous research [16] studied the behavior of such a PbO-SiO_2-MgO slag in contact with the same refractory brick under isothermal conditions. The goal of this work is to determine the effect of the temperature gradient on the infiltration behavior of the slag, the formation of reaction phases and the modification in slag composition.

2 Experimental procedure

The refractory samples were tested under a temperature gradient using a newly designed experimental setup, shown in Fig. 1. It consists of a refractory sample, a cooling probe and a crucible containing liquid slag. The cylindrical refractory samples, having a diameter of 30 mm and a height of 70 mm, were machined out of commercially available fused grain rebonded magnesia-chromite bricks. The global composition, detailed description of the microstructure and the composition of all the present phases have been previously described by the present authors [16]. In the center of the samples a cylindrical hole was drilled with a diameter of 10 mm and a depth of 60 mm. In this hole a cold finger probe was inserted and fixed to the refractory using castable alumina, thereby also ensuring no air is left between the refractory sample and the cooling probe, as this would drastically

decrease the heat removal to the probe. The cooling probe consists of two concentric stainless steel tubes; the external tube has a diameter of 9.5 mm (3/8 inch) and is closed at the bottom while the interior tube has a diameter of 6.35 mm (1/4 inch). Air was blown at a flow rate of 100l/h through the interior tube and released through the gap between both tubes, thereby removing heat from the probe surface and cooling the refractory sample. The obtained temperature gradient was measured at 3 different positions: (1) in a groove in the surface of the cooling probe, (2) midway inside the refractory sample (5 mm from the cooling probe surface) and, finally, (3) in a groove in the surface of the refractory sample in contact with the liquid slag. K type thermocouples (1 mm diameter) were placed at a depth of 4 cm (taken from the top of the sample) for all three positions. 5 mm from the hot face a hole was drilled to place the thermocouple in. Because of the depth it was impossible to have the same thickness as the thermocouple. The diameter of the created hole was approximately 2 mm. For the thermocouples at the hot face and the cooling probe the grooves were 1 mm, the same size as the thermocouples. The thermocouples were positioned non-collinear to ensure that the measurements did not influence each other. The local replacement of refractory phases by a hole and thermocouple with a different conductivity and heat capacity could otherwise influence the other temperature measurements. For the same reason the sample taken for investigation of the microstructure was taken at the opposite side of the sample to the thermocouples.

The PbO-SiO_2-MgO slag was produced by mixing pure oxides (Alfa Aesar, purity level of 99.9 wt%) powders in the desired ratio (54 mole% PbO, 41 mole% SiO_2 and 5 mole% MgO) to a total weight of 3 kg. It was heated in open air at a rate of 40 °C/hour in an MgO crucible using a resistance furnace until a temperature of 1100 °C was reached. After 1100 °C was obtained, the refractory sample, attached to the cold finger probe, was slowly lowered into the furnace. It was kept above the liquid bath for at least 30 min while air was blown through the probe, creating a temperature gradient over the sample before the sample was partially submerged into the liquid slag bath. After the required reaction time the sample was taken out of the bath and quenched in water in order to preserve the high temperature microstructure and composition in the best possible way. The time between removal of the sample from the liquid bath and quenching was approximately 2-3 s. Three different reaction times were tested: 15 min, 1 h and 2.5 h.

After the experiment a sample was taken from the refractory finger for microstructural investigation. The location of sampling is shown in Fig. 1. Before this sample was analyzed it was embedded in an epoxy resin and polished. After coating the sample with a conducting carbon layer, both its microstructure and the composition of the different phases were analyzed using a fully quantitative EPMA-WDS (JEOL JXA-8530F) system. It was operated using an acceleration voltage of 15 kV and a probe current of 15 nA. The oxygen content was not measured directly; instead the oxidation state of the element was selected a priori. Although both Fe^{2+} and Fe^{3+} can be present in the liquid slag and solid phases in the sample under consideration here, "Fe_2O_3" was selected for presentation purposes only.

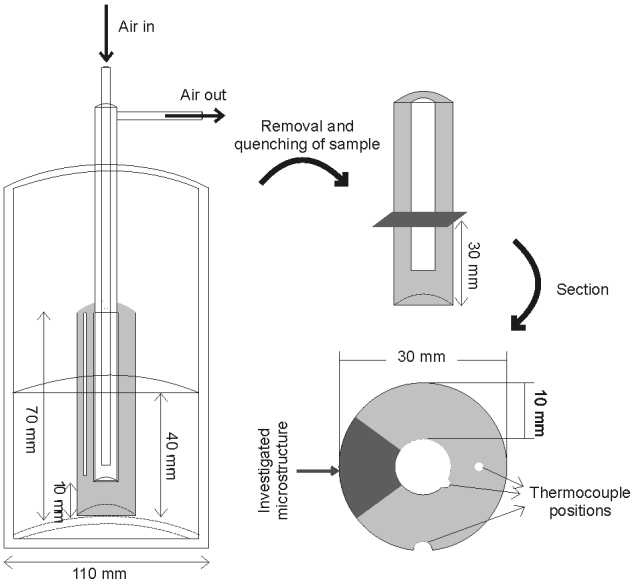

Fig. 1: Schematic representation of the experimental setup and a top view of the sample showing the position of the thermocouples.

3 Results

3.1 Temperature measurements

Fig. 2 shows the variation of the temperature at 3 different positions in the refractory sample as a function of the submersion time. After contact with the slag, the temperature at the slag-sample interface (called the hot face) and 5 mm from the hot face decrease with time, while the temperature at the cooling probe surface increases. All three temperatures level off with time. The average temperatures (taken from 5000 s onwards) during the steady state are: 740 °C for the cold face, 982 °C 5 mm from the hot face and 1078 °C at the hot face.

Using these measured values the temperature throughout the entire sample can be estimated using the heat transport equation, which in cylindrical coordinates (r, φ, z) is given below:

$$\frac{1}{r}\frac{\partial}{\partial r}\left(rk\frac{\partial T}{\partial r}\right)+\frac{1}{r^2}\frac{\partial}{\partial \varphi}\left(k\frac{\partial T}{\partial \varphi}\right)+\frac{\partial}{\partial z}\left(k\frac{\partial T}{\partial z}\right)+\ q_{gen}=\rho c_p\frac{\partial T}{\partial t} \qquad (1)$$

Where q_{gen} is heat generation, k heat conductivity, ρ density and c_p heat capacity. Equation 1 can be simplified by only considering the steady state (∂T/∂t=0) and by making the following assumptions: (1) the heat generated (or used) by reactions between the infiltrated slag and the refractory brick is negligible compared to the heat removed by the cooling probe (q_{gen}=0) and (2) the heat conductivity (k) of the sample is independent of temperature. The geometry of the sample can also be used by assuming (3) the sample is homogeneous and the effect of the different phases in the microstructure is thus not taken into account, which for a cylindrical sample means ∂T/∂φ=0. Finally, (4) the sample is considered to be sufficiently long that the temperature in the investigated part of the sample can be considered to be independent of the height (∂T/∂z=0). Equation 1 then becomes:

$$\frac{1}{r}\frac{\partial}{\partial r}\left(r\frac{\partial T}{\partial r}\right)=0 \quad (2)$$

Solving of this equation gives the temperature as a function of position:

$$T(r)=C_1\,ln(r)+C_2 \quad (3)$$

Equation 3 requires 2 boundary conditions to determine C1 and C2. Using the measured steady state temperatures at the hot (T_{HF}) and cold face (T_{CF}) this gives:

$$T(r)=T_{CF}+\frac{T_{HF}-T_{CF}}{ln\left(\frac{r_{HF}}{r_{CF}}\right)}\,ln\left(\frac{r}{r_{CF}}\right) \quad (4)$$

The measured sample thickness from Fig. 3 (described in the next section) is used as the difference between the cold face radius (r_{CF}=5 mm) and the hot face radius (r_{HF}). The obtained temperature profile is used below together with the slag measurements at each position.

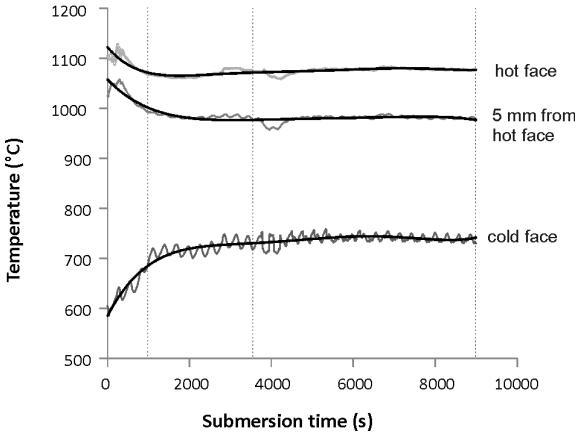

Fig. 2: Temperature data at different positions in the sample. The bath temperature was kept at 1100 °C. The curves in black are fitted polynomials (order 5) for the experimentally obtained data (shown in gray). The dotted vertical lines indicate the times when samples were taken.

3.2 Microstructure

Fig. 3 shows a microstructure of the cross section from the liquid bath (hot face) to the cooling probe (cold face) as well as detailed images at different positions inside each sample. The liquid slag, seen as the white phase in Fig. 3, forms a thin layer at the hot face but also infiltrates the refractory samples; only the first 1.5 mm for the 15 min sample, while the samples after 1 h and 2.5 h are both completely infiltrated. The cold face of the 15 min sample is identical to the microstructure of an unreacted fused grain rebonded magnesia-chromite brick, consisting of primary chromite spinel (PC, $[Mg,Fe^{2+}][Cr,Al,Fe^{3+}]_2O_4$) and fused grains (FG), which consist of chromite spinel particles in a periclase (MgO) matrix [1, 17, 18]. These phases remain clearly visible inside the infiltrated parts of all samples. The slag infiltrates the pores, which are still clearly visible in the unreacted part of the 15 min sample. Some pores and cracks (C) are also present in the infiltrated part of the brick and are

formed either by (1) thermal shock during quenching, (2) mechanical load during sample preparation or (3) were closed off from the slag during infiltration.

Detailed images of the hot face (Fig 3. a-c) show that for all samples forsterite (Mg_2SiO_4) grains are present inside the liquid bath near the refractory sample. Inside the samples this phase also forms grains between the periclase of the fused grains and the liquid slag, but it is not detected in contact with primary or secondary chromite spinel grains. Finally, for the 1 h and 2.5 h samples, melilite (M, $[Ca,Pb]_2[Fe,Mg,Al][Si,Al,Fe]_2O_7$) is detected near the cold phase (between 7-10 mm from the bath). At the same position some forsterite particles are also present, although they are much smaller than the melilite grains.

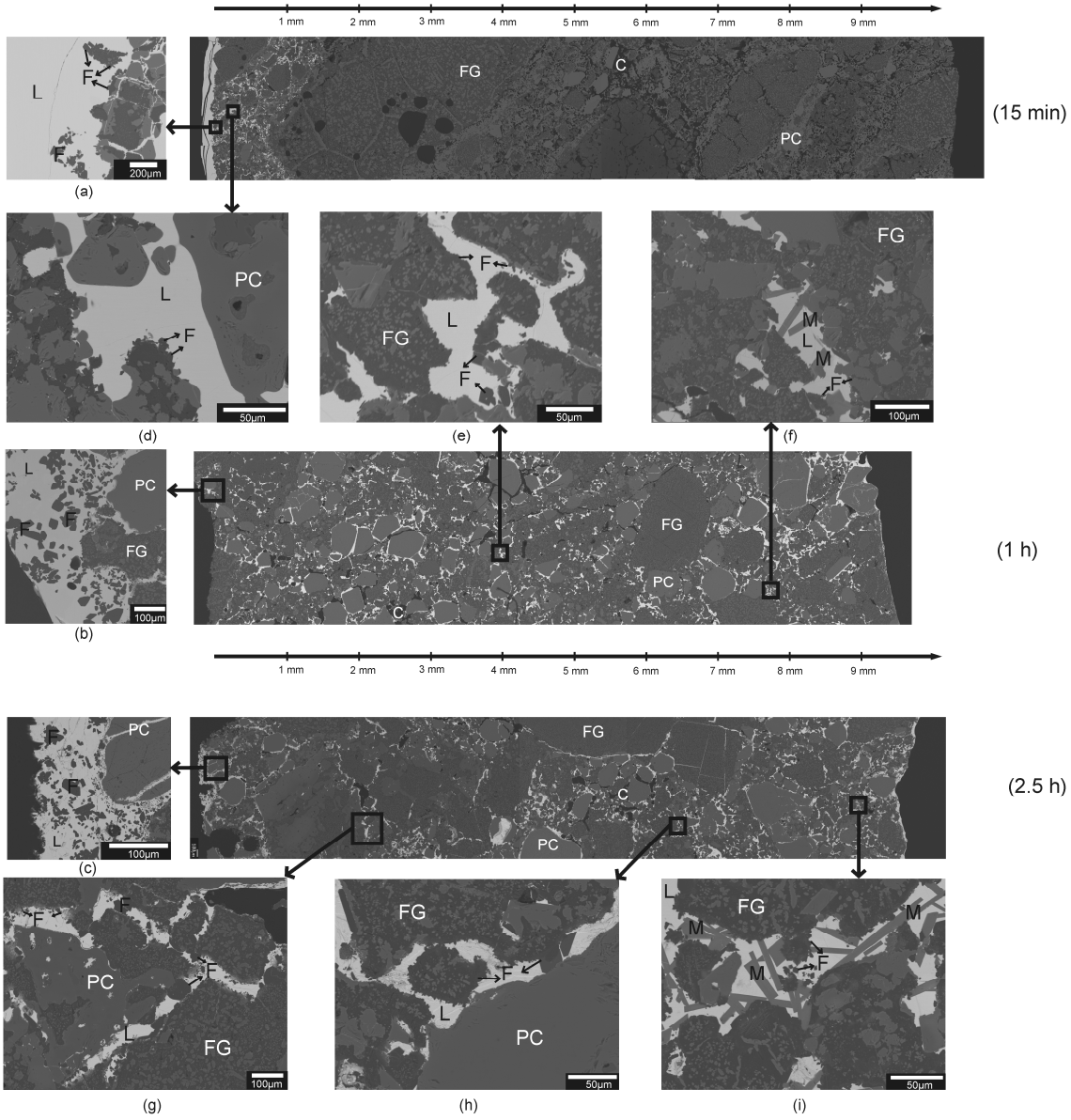

Fig. 3: BSE images of the microstructure showing a cross section after 15 min, 1 h and 2.5h as well as detailed images at the hot face (a-c) and deeper inside the samples (d-i). With FG: fused grain, PC: primary chromite, L: liquid slag during experiment, C: cracks and pores, F: forsterite and M: melilite.

The forsterite grains at the hot face (Fig. 3 a-c) appear to be larger than inside the sample and, furthermore, their size appears to increase with time, although size quantification of these grains inside the sample is difficult based on the images, because forsterite has the same BSE brightness as periclase. The forsterite amount is therefore determined by WDS mapping of several rectangular areas of 400 µm by 1300 µm, taken between the hot and the cold face of the sample. The first analysis is taken with the center of the measured area at the contact interface between slag and sample with the shortest side of the rectangle in the direction towards the cold face. For the subsequent analyses, the measurement area is always moved an additional 1 mm towards the cold face. For each area a WDS analysis is performed every micron for 10 ms. By analyzing the results at each point it is possible to determine which phase is present: forsterite (when both MgO and SiO_2 are detected), slag (based on the presence of PbO), chromite (when Cr_2O_3 is detected) or periclase (only MgO). Based on this result, the forsterite area fraction is calculated for each measured area.

Most of the detected forsterite formed after reaction between the slag and the refractory sample. The presence of larger grains in the measured area will lead to a lower forsterite area fraction as there is less slag and therefore less reaction leading to new forsterite. As seen in Fig. 3, the forsterite only formed when the slag is in contact with periclase and not in contact with chromite spinel phases. When a lot of these chromite grains are present in the analyzed area, the detected forsterite amount is also lower. To identify the effect of the temperature gradient and the reaction time on the forsterite formation, the effect of the local microstructure is countered by scaling the forsterite amount to the reaction surface. Only the periclase-slag and forsterite-slag interfaces are taken into account for the reaction surface. The result is given in Fig. 4, showing that the detected amount of forsterite increases with time and that this increase is larger closer to the hot face of the sample.

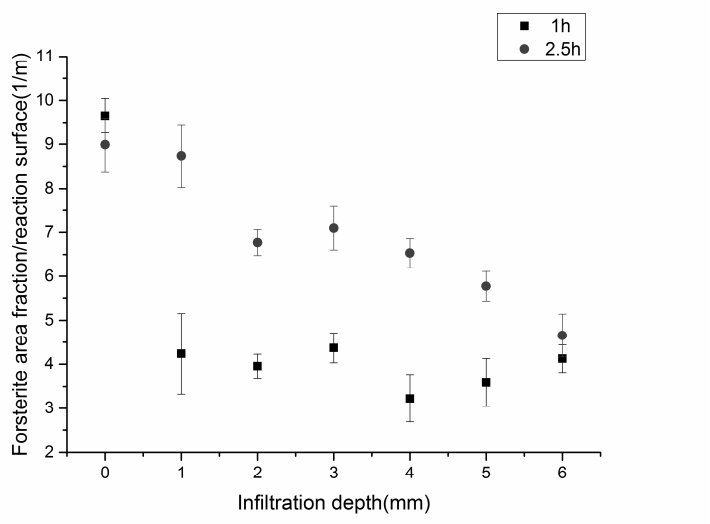

Fig. 4: The measured amount of forsterite per reaction surface (slag-MgO interface and slag-forsterite interface) for two different reaction times.

3.3 Slag composition as a function of position

The composition of the infiltrated slag is measured with EPMA-WDS at different positions inside each sample. Fig. 5 shows the concentrations of the main slag components (PbO, SiO_2 and MgO) with position inside the sample together with the temperature profile measured and estimated as described above with reference to equation (4). The PbO content of the slag varies in the opposite direction with respect to the SiO_2 and MgO content of the slag. The PbO content increases towards the cold face and this increase is most pronounced in the first 1-2 mm of the sample. The PbO content levels off deeper inside the sample, reaching a constant value 3 mm from the hot face. With increasing reaction time this constant value increases. In the final millimeter of the 2.5 h sample, the PbO content decreases again.

Fig. 5 only showed the variation of the main slag components. However, some other components are also detected, which dissolved from the refractory phases into the liquid slag. Due to the large dataset, an average composition is given in Table 1. This average has been taken for 1 mm sections, except for the first 3 mm where the average of a 0.5 mm section is taken due to the large change in composition with position. For each section at least 6 points were used to calculate the average. Table 1 shows that the concentration of the spinel components (Cr_2O_3, Fe_2O_3 and Al_2O_3) in the liquid slag all increase towards the cold face of the sample.

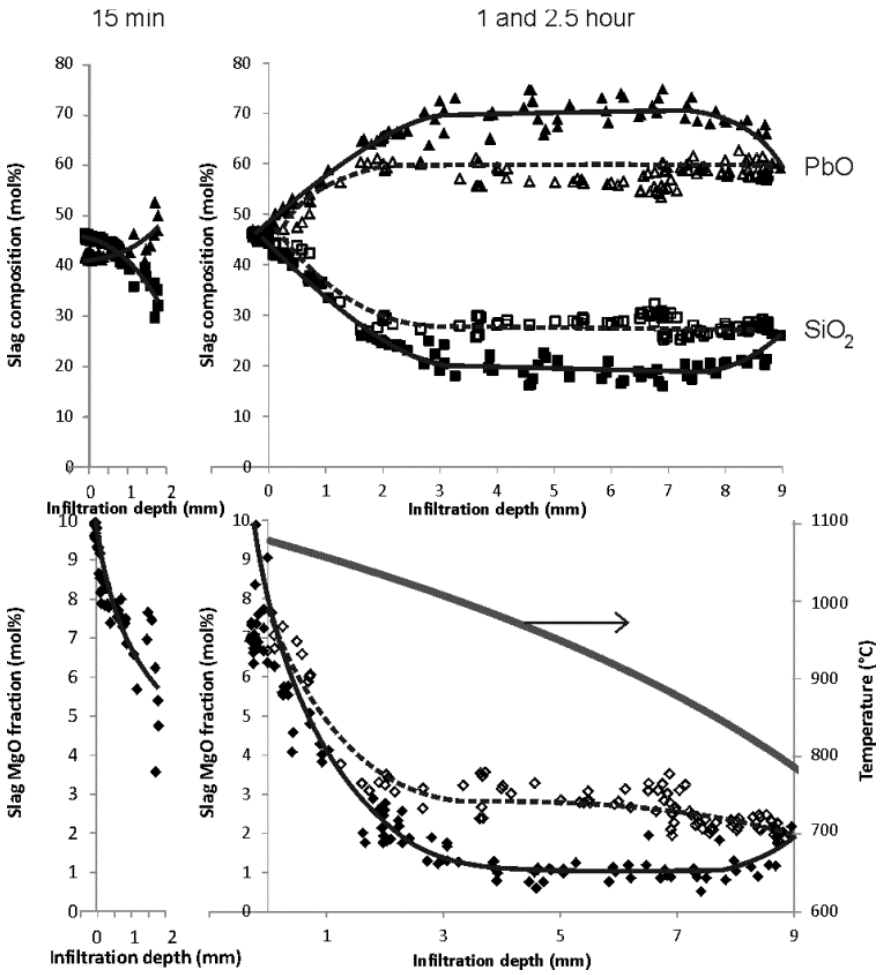

Fig. 5: Concentration of the major slag components (PbO, SiO_2, MgO) as a function of position and reaction time. (1h open markers and dotted lines and 2.5h filled markers and full lines) obtained using EPMA-WDS.

Table 1: Composition of the slag measured using EPMA-WDS and calculated temperature at different positions for the tested reaction times.

Section	Distance From bath [mm]		15 min MgO	SiO_2	Cr_2O_3	"Fe_2O_3"	PbO	Al_2O_3	CaO
A	bath		9.8	45.7	0.0	0.1	42.0	1.2	1.2
B	0-0.5		8.4	45.4	0.3	0.2	42.0	1.6	2.1
C	0.5-1		7.6	43.2	0.6	0.4	42.5	1.4	4.3
D	1-1.5		6.7	38.2	1.2	1.0	43.3	1.6	8.0
E	1.5-2		5.5	33.9	2.1	1.2	48.0	1.7	7.5

Section		Calculated temperature	1 h MgO	SiO_2	Cr_2O_3	"Fe_2O_3"	PbO	Al_2O_3	CaO	2,5 h MgO	SiO_2	Cr_2O_3	"Fe_2O_3"	PbO	Al_2O_3	CaO
A	bath	1078	6.7	44.3	0.0	0.1	47.6	0.9	0.4	7.2	45.8	0.1	0.1	46.3	0.3	0.2
B	0-0.5	1072	7.0	44.2	0.0	0.2	47.3	0.9	0.4	5.7	41.5	0.2	0.7	50.7	0.8	0.3
C	0.5-1	1061	6.3	40.8	0.2	0.7	50.3	1.1	0.6	4.4	36.8	0.6	1.1	55.3	1.3	0.5
D	1-1.5	1049	3.8	32.7	0.4	2.2	56.3	3.1	1.5	4.1	33.5	0.1	1.3	58.8	1.3	0.8
E	1.5-2	1037	3.2	27.2	0.2	2.9	60.6	3.2	2.7	2.2	25.2	0.3	2.8	64.7	2.2	2.5

F	2-2.5	1024	3.3	29.2	0.3	2.8	59.6	2.7	2.2	2.2	24.1	0.3	2.8	66.0	2.1	2.5
G	2,5-3	1011	2.9	27.2	0.4	3.4	60.2	2.9	3.0	1.4	21.6	0.7	3.8	68.8	1.6	1.9
H	3-4	990	3.0	28.1	0.2	3.5	58.0	3.3	3.9	1.3	20.5	0.8	4.9	68.8	1.7	2.0
I	4-5	960	2.5	28.4	0.2	3.5	58.2	3.1	4.1	0.9	18.8	1.0	5.0	70.9	1.6	1.8
J	5-6	927	2.8	28.8	0.4	3.6	56.4	3.3	4.6	1.0	19.3	1.1	4.9	69.9	1.7	2.0
K	6-7	889	2.5	28.9	0.6	3.7	56.5	3.1	4.7	1.1	17.6	1.1	4.6	71.9	1.6	2.1
L	7-8	847	2.4	26.9	0.9	4.1	58.7	3.1	4.0	1.1	19.2	1.2	4.7	70.0	1.6	2.2
M	8-9	798	1.7	27.7	1.0	4.3	58.6	2.5	4.1	1.5	22.7	1.5	4.5	64.8	1.9	3.0
N	9-9.5	755								2.3	29.8	1.3	4.3	55.4	2.3	4.5

To achieve a better insight into the mechanisms responsible for the changing slag composition the results from Table 1 are projected onto a PbO-SiO_2-MgO phase diagram in Fig. 6, by normalizing the slag composition in Table 1 to only MgO, SiO_2 and PbO. This phase diagram is created using the phase equilibria results for the liquidus lines of the forsterite primary phase field of the PbO-MgO-SiO_2 system obtained from Chen et al. [19] for 3 different temperatures (1100, 1000 and 900 °C). Interpolation of these values gives the liquidus lines for each temperature in Fig. 6 (full lines). The liquidus lines are further extrapolated using the data from Scheunis et al. [16] (dotted lines). The local temperature in the center of each section is calculated using equation 4 and is provided in Table 1, making it possible to check how the slag composition varies with position in the sample with respect to the liquidus lines. The slag composition inside the refractory moves towards the PbO corner of the phase diagram with time and infiltration depth, while all points stay on the liquidus lines.

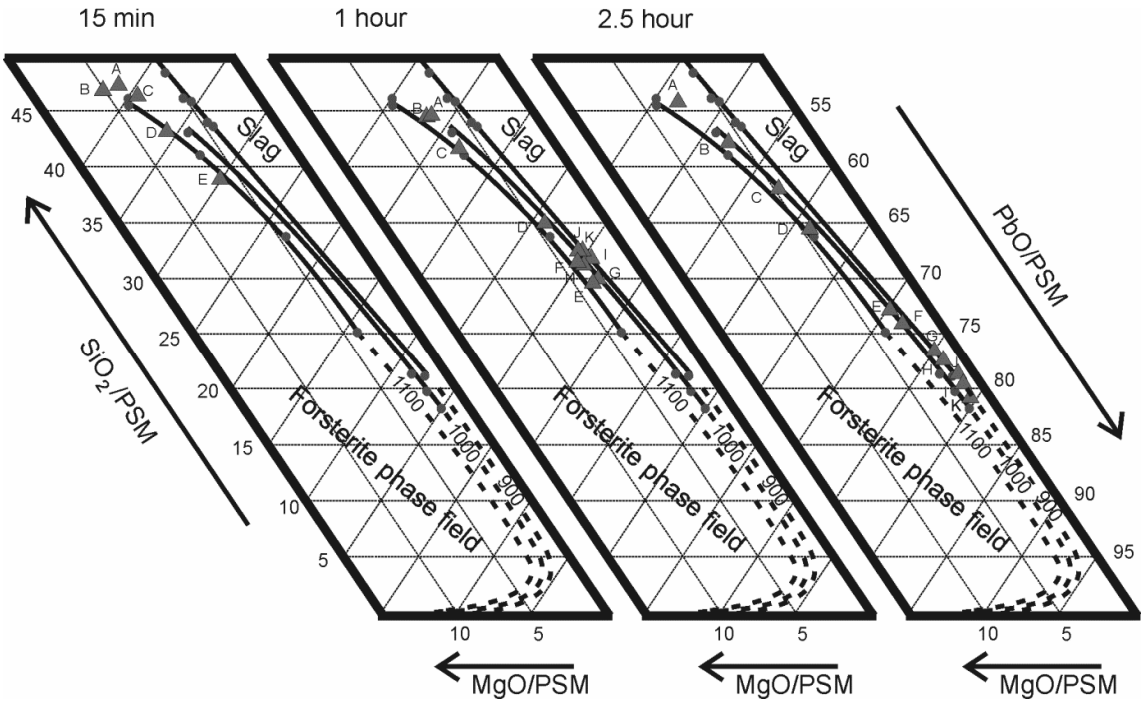

Fig. 6: Projection of the slag composition in mole % on the PbO-MgO-SiO_2 ternary phase diagram for the different section of the samples given in Table 1 at 3 different reaction times (15 min, 1 h and 2.5 h). The liquidus lines at 1100 °C, 1000 °C and 900 °C are interpolated (full lines) and extrapolated (dotted lines) based on the phase equilibria results (●) obtained from Chen et al [19].

4 Discussion

To minimize the refractory wear it is vital to understand how the degradation mechanism changes inside the lining. The degradation in the interior of the lining is controlled by local equilibrium [20], which is the equilibrium between the refractory phases and the local slag composition at the local temperature. It is thus essential to know how the slag composition and temperature vary with position. For a sample under a temperature gradient not only the slag composition and temperature, but also the infiltration behavior varies with position and time. The study of these effects is further complicated as they influence each other. Therefore, the local temperature, infiltration behavior and slag composition are discussed separately, starting with the variation in local temperature.

4.1 Local temperature

As seen in the microstructural images (Fig. 3), the slag infiltrates the refractory during the first hour of reaction, while the measured temperature inside the sample varies continuously (Fig. 2). The temperature variation is, therefore, probably due to a difference in thermal conductivity between the infiltrated and original refractory part of the sample due to the replacement of entrapped air in the pores by more conductive slag. After full infiltration of the sample (1 h reaction time in Fig. 3) the measured temperatures reach a steady state condition with a smaller temperature difference between the hot and cold face, further supporting the hypothesis that the infiltration of slag causes the thermal conductivity to increase. The local temperature throughout the sample is calculated during this steady state. The simplifications made to do this can be evaluated by comparing the measured (982 °C) and calculated (944 °C) temperature values 5 mm from the hot face. The difference is probably due to two main causes: (1) the assumption of a temperature independent thermal conductivity of the infiltrated refractory is not valid for the large temperature range between the hot and cold face of the sample, resulting in an error in the calculated value and, probably the most important effect is (2) the size of the hole for the thermocouple at 5 mm from the hot face, which as a diameter of approximately 2 mm, causes an error in the measured value. It is assumed that the effect of the latter is larger than the effect of the former. A variation of the measurement position of 1.5 mm already causes the calculated temperature to increase to 990 °C instead of the 944 °C calculated at 5 mm from the hot face. For this reason the calculated values are used in Table 1.

4.2 Slag composition

The slag composition is a function of the infiltration behavior and the local temperature. A slow infiltration rate leads to a longer reaction time between slag and refractory before the slag infiltrates deeper into the lining, while the temperature controls the thermodynamics and kinetics of all reactions. The local slag composition (Fig. 5) and the detected forsterite amount (Fig. 4) are therefore closely related. For the studied system, the slag composition changes due to removal of SiO_2 by the formation of forsterite:

$$2MgO_{ref} + SiO_{2slag} \rightarrow Mg_2SiO_{4ref} \quad (5)$$

This reaction continues until equilibrium is reached between the slag, forsterite and periclase phases. Based on Fig. 6, the slag equilibrium composition is not reached for any of the measurements. From a

thermodynamic point of view, reaction 5 will therefore continue. This explains why the detected forsterite amount increases with time, while the SiO_2 decreases. This change is most pronounced near the hot face where the local temperature and thus the reaction rate is higher.

Based on the PbO-SiO_2-MgO phase diagram (Fig. 6), the MgO content in the liquid slag follows the liquidus lines, indicating that the liquid is in equilibrium with the newly formed forsterite. Deviations from the liquidus lines can be caused by (1) imperfect quenching of the sample, due to its large size, (2) the effect of the minor components (see Table 1), which up till now has been neglected or (3) the limited size of the measurement areas in the sample (1–5 µm), leading to some overlap of the X-ray excitation volume during the EPMA measurements with the surrounding (MgO rich) phases.

4.3 Infiltration behavior

The infiltration behavior is controlled by both the slag composition and the local temperature. For an isothermal non-reactive liquid the infiltration depth increases with √t, according to the following equation [21]:

$$l = \sqrt{\frac{r\sigma \cos\theta t}{2\eta}} \tag{6}$$

where l is the infiltration depth, r the pore radius, σ the surface tension of the liquid slag, θ the contact angle between the liquid slag and the refractory, t the reaction time and η the viscosity of the liquid slag.

Without reaction, the presence of a temperature gradient will increase the viscosity of the liquid deeper inside the sample, thereby slowing down the infiltration rate compared to the isothermal case. Most slag systems, however, react with the refractory, changing the liquid composition. Two cases can be identified based on the slag components being removed: (A) the reaction between the liquid and the refractory phases hinders further infiltration [21] or (B) the change in liquid composition accelerates the infiltration [16].

Fig. 7 shows the time dependency of the infiltration depth as well as the variation of the viscosity with position, with and without the presence of external cooling. For an isothermal, non-reactive slag the viscosity remains constant over the entire sample. According to equation 5 the infiltration depth thus increases with √t. The slag's viscosity increases exponentially with the inverse temperature. The infiltration of the slag will therefore go much slower in a gradient and will also stop before full infiltration of the sample when the slag solidifies inside the sample. When the slag reacts with the refractory phases, components are selectively removed from the infiltrating liquid, rendering the slag composition a function of the infiltration depth. When this reaction leads to an increase of the slag's viscosity (case A) with depth, the infiltration rate will be slower than for a non-reactive slag system. The additional application of a temperature gradient will increase the viscosity even further resulting in an even slower infiltration behavior.

Finally, the reaction can reduce the slag viscosity (case B), leading to a faster slag infiltration compared to a non-reactive system. A temperature gradient will increase the viscosity and decrease the infiltration rate, although the rate may still be higher than the isothermal non-reactive case, if the effect of reaction has a bigger influence on the viscosity than the temperature. Towards the cold face the changes in the slag composition will be limited, due to the slower kinetics, and the change in

viscosity is dominated by the temperature. It is therefore still possible to stop the infiltration of the slag if the temperature gradient is sufficiently large.

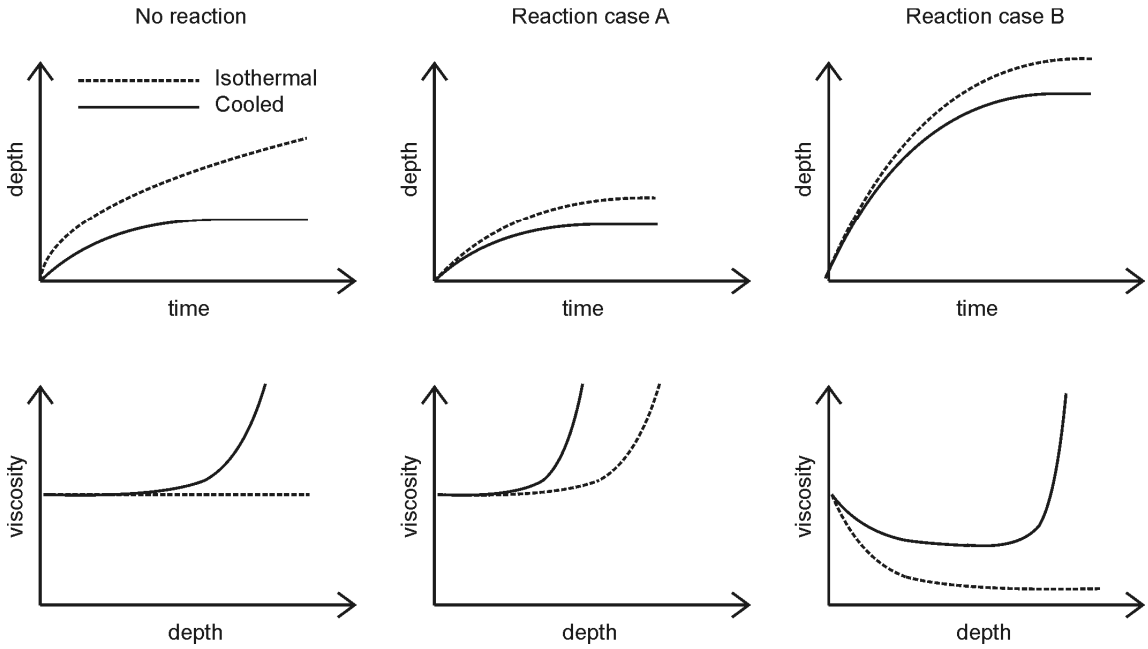

Fig. 7: Conceptual description of the effect of a temperature gradient on the infiltration depth with time for three different slag systems: (1) without reaction with the refractory phases, (2) reaction with the refractory phases hindering further infiltration and (3) reaction accelerating infiltration of the liquid. For all three cases the isothermal situation (dotted lines) is compared to the situation when a temperature gradient is applied (full lines).

The viscosity of the liquid slag as a function of depth for all samples is calculated using the FactSage viscosity module, which for PbO-SiO_2 slags has been optimized by Kim et al. [22]. The viscosity is calculated based on the local slag composition and temperature, both given in Table 1. The result of the calculations is shown in Fig. 8. Despite the decreasing temperature, the viscosity significantly drops in the first 2 mm of the sample due to the changing liquid composition. At the cold face the viscosity increases again due to the limited change in slag composition and is thus controlled by the decrease in temperature. This matches reaction case B discussed in Fig. 7. With time the reaction between the refractory phases and the liquid continues, causing the slag composition to change, in turn leading to a drop in viscosity from 1 h to 2.5 h reaction time.

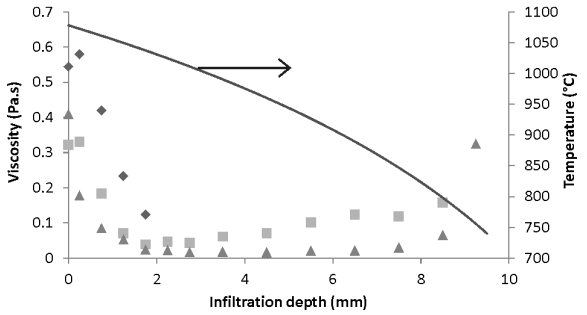

Fig. 8: The temperature and viscosity for 3 reaction times (♦: 15 min, ■:1 h and ▲: 2.5 h) as a function of the distance from the slag-refractory interface. The calculations are done using the FactSage viscosity module [23, 24] based on the average composition and temperature given in Table 1.

Equation 6 shows that the infiltration behavior depends on several slag properties (viscosity, surface tension and contact angle with the refractory phases), all changing with slag composition. For the studied PbO-SiO_2-MgO slag, the infiltration depth is calculated for the minimum and the maximum values for each slag property, while all other parameters in equation 6 are kept constant. In this way the relative significance of the slag properties on the infiltration behavior can be determined. The viscosity varies between 0.579 Pa.s (0.25 mm from the hot face after 15 min) and 0.039 Pa.s (2 mm from the hot face after 1 h), resulting in a ratio of 3.9 for both infiltration rates. To estimate the effect of the surface tension of the slag, the available data for the PbO-SiO_2 system at 850 °C are used [25]. The PbO content of the slag varies between 50 mole% (218.6 10^{-3} N/m) up to 70 mole% (175.2 10^{-3} N/m), resulting in a ratio of 1.1 for the infiltration rate. For the contact angle (θ) no data are available. Because the slag completely wets the pores for all compositions (as seen in Fig. 3), cos θ can be considered close to 1, which is a common assumption in refractory research [5]. No large influence on the infiltration behavior is therefore expected. The slag viscosity significantly influences the infiltration behavior. To a first approximation the infiltration behavior can be studied by only considering the effect of the viscosity. The studied PbO-SiO_2 slag system is clearly an example of a case B reaction discussed in Fig. 7.

Equation 6 is only valid if all parameters remain constant during the reaction. A more accurate description of the infiltration behavior of the liquid slag requires the solution of the following equation:

$$\frac{dl}{dt} = \frac{r\sigma \cos\theta}{4\eta l} \qquad (7)$$

Using equation 7, the increase in infiltration depth (Δl) is determined after each time step (Δt) using the local values for the viscosity (η), contact angle (θ) and surface tension (σ). All these parameters, however, depend on both the liquid composition and the local temperature. In order to determine the temperature distribution for a partially infiltrated sample, the heat equation (equation 1) has to be solved which requires the thermal conductivity of an infiltrated brick, which, to the best of the authors' knowledge, is not available. Predicting the local slag composition is also impossible as both the reaction kinetics of the phase formation, causing the compositional change, and the local temperature are unknown. Due to these practical difficulties, a full description of the infiltration as a function of time has not been performed.

4.4 Effect of external cooling on chemical degradation

External cooling is applied in industrial furnaces to limit refractory wear by (1) reducing the dissolution of the refractory components in the slag, (2) freezing the slag in the lining and thus reducing the exposed part of the lining and (3) by lowering the reaction kinetics, reducing the densification by new phases being formed. Each of these three effects is discussed below for the studied PbO-SiO_2-MgO system.

The MgO content of the liquid slag decreases towards the cold face of the sample (Fig. 5). According to the PbO-SiO_2-MgO phase diagram (Fig. 6) the decrease in MgO solubility of the liquid can be due to both a lower temperature and/or a lower SiO_2 content in the liquid. By comparing the results in Fig. 5 with those from an isothermal study on the interaction between a PbO-SiO_2 slag and a refractory sample [16], it is seen that the MgO content of the liquid decreases faster and closer to the hot face for the isothermal case. The faster SiO_2 removal (by faster forsterite formation) thus appears to have a larger effect on the MgO solubility than the decreasing temperature.

The infiltration rate decreases due to the applied temperature gradient, but this effect is (partially) countered by the change in liquid composition over time. Eventually the decreasing temperature will freeze the slag inside the refractory lining. The isothermal study showed that the slag reaches a composition of almost pure PbO in the interior of the sample after 15 min reaction time. Based on the result for this isothermal case, one would expect the slag in a temperature gradient to freeze below the melting point of PbO (880 °C). This is, however, not the case in the performed experiment. Due to the lower temperatures (and slower kinetics) towards the cold face, the liquid does not remove all the SiO_2 before the infiltration is arrested and the slag will only freeze at its lowest eutectic temperature (717 °C for a 25 mole% SiO_2-75 mole% PbO slag [26]). The temperature when the liquid freezes, thus, depends on the liquid composition, which in turn, depends on the slag composition and, hence, on the SiO_2 removal. The SiO_2 in turn depends on the forsterite growth (depends on the temperature) and the specific reaction surface (depends on the pore size distribution).

The application of external cooling clearly lowers the kinetics (Fig. 5) and thus the forsterite formation (Fig. 4) and the densification this may cause. The presence of large amounts of forsterite can lead to failure of the lining, a mechanism referred to as forsterite bursting [27]. The risk for forsterite bursting therefore decreases when external cooling is applied.

The interaction between a synthetic PbO-SiO_2-MgO slag and a magnesia-chromite refractory sample has previously been studied under isothermal conditions [16], showing the same forsterite formation as in this paper. For both the isothermal and temperature gradient experiments the SiO_2 content decreased towards the center of the sample due to this forsterite formation. For the isothermal case, the SiO_2 content of the slag reaches a value of 5 mole% in the center of the sample, considered to be the equilibrium concentration of the slag in contact with periclase and forsterite. At lower temperatures, the SiO_2 equilibrium concentration in the slag will be even lower. Fig. 6 clearly shows that this low SiO_2 content has not been reached yet and the formation of forsterite is expected to continue.

5 Conclusion

A newly developed experimental setup has been used to examine the effect of a temperature gradient on the reaction between a synthetic PbO-SiO_2 slag and a porous magnesia-chromite brick. Based on the results the following conclusions can be drawn:

- The temperature inside the sample changes with infiltration depth of the liquid. The replacement of air in the pores by more conductive slag increases the thermal conductivity of the infiltrated part of the sample. As the infiltration progresses the difference in thermal conductivity between the infiltrated and original part of the lining leads to a continuous temperature variation in the sample. After full infiltration, the temperature gradient remains constant, but is less steep compared to the original sample.
- The reaction between the slag and the refractory changes with temperature. Higher temperatures lead to faster kinetics of forsterite formation, and thus faster SiO_2 removal from the liquid slag, while in the cooler part of the sample both the phase formation and change in slag composition occur more slowly.
- The infiltration rate changes with slag composition and temperature. At the hot face the effect of the slag compositional change is most dramatic, decreasing the SiO_2 content in the liquid slag and leading to a drop in the liquid's viscosity. Near the cold face the removal of SiO_2 is limited and the change in viscosity is determined by the decreasing temperature.

Whether the applied gradient has a beneficial effect on the refractory lifetime depends on the studied slag system and on the dominant refractory degradation mechanisms causing the wear. For the studied PbO-SiO_2 slag, applying a temperature gradient limits densification in the lining but also leads to a relatively high MgO solubility of the liquid slag near the hot face, as the removal of SiO_2 is hindered by slower kinetics inside the sample.

6 Acknowledgements

This research was supported by the Agency for Innovation by Science and Technology in Flanders and by Umicore (IWT Baekeland mandate 100700). We also gratefully acknowledge support from the Hercules Foundation (project ZW09-09) for the use of the FEG-EPMA system.

7 References

1. Malfliet A., Lotfian S., Scheunis L., Petkov V., Pandelaers L., Jones P. T. and Blanpain B., *Degradation mechanisms and use of refractory linings in copper production processes: A critical review.* Journal of the European Ceramic Society, 2014. **34**(3): p. 849-76.
2. Gregurek D., Reinharter K., Majcenovic C., Wenzl C. and Spanring A., *Overview of wear phenomena in lead processing furnaces.* Journal of the European Ceramic Society, 2015(0).
3. Gregurek D., Majcenovic C., Spanring A. and Kirschen M., *Wear phenomena of basic brick linings in the copper industry*, in *Copper*2013: Santiago de Chile. p. 473-84.
4. Braulio M. A. L., Zinngrebe E. W., van der Laan S. R. and Pandolfelli V. C., *Steel ladle well block post mortem analysis.* Ceramics International, 2012. **38**(2): p. 1447-62.
5. Lee W. and Zhang S., *Melt corrosion of oxide and oxide–carbon refractories.* International Materials Reviews, 1999. **44**(3): p. 77-104.

6. Gregurek D., Ressler A., Reiter V., Franzkowiak A., Spanring A. and Prietl T., *Refractory wear mechanisms in the nonferrous metal industry: testing and modeling results.* JOM: The Journal of The Minerals, Metals & Materials Society (TMS), 2013. **65**(11): p. 1622-30.
7. Campforts M., Blanpain B. and Wollants P., *The importance of slag engineering in freeze-lining applications.* Metallurgical and Materials Transactions B-Process Metallurgy and Materials Processing Science, 2009. **40**(5): p. 643-55.
8. Campforts M., Jak E., Blanpain B. and Wollants P., *Freeze-lining formation of a synthetic lead slag: Part I. Microstructure formation.* Metallurgical and Materials Transactions B-Process Metallurgy and Materials Processing Science, 2009. **40**(5): p. 619-31.
9. Verscheure K., Campforts M., Verhaeghe F., Boydens E., van Camp M., Blanpain B. and Wollants P., *Water-cooled probe technique for the study of freeze lining formation.* Metallurgical and Materials Transactions B-Process Metallurgy and Materials Processing Science, 2006. **37**(6): p. 929-40.
10. Fallah-Mehrjardi A., Hayes P. C. and Jak E., *Investigation of freeze-linings in copper-containing slag systems: Part I. Preliminary experiments.* Metallurgical and Materials Transactions B-Process Metallurgy and Materials Processing Science, 2013. **44**(3): p. 534-48.
11. Jansson J., Taskinen P. and Kaskiala M., *Freeze-lining formation in continuous converting calcium ferrite slags. I.* Canadian Metallurgical Quarterly, 2013. **53**(1): p. 1-10.
12. Kaneko T. K., Bennett J. P. and Sridhar S., *Effect of temperature gradient on industrial gasifier coal slag infiltration into alumina refractory.* Journal of the American Ceramic Society, 2011. **94**(12): p. 4507-15.
13. Kaneko T. K., Zhu J., Howell N., Rozelle P. and Sridhar S., *The effects of gasification feedstock chemistries on the infiltration of slag into the porous high chromia refractory and their reaction products.* Fuel, 2014. **115**: p. 248-63.
14. Kaneko T. K., Zhu J., Thomas H., Bennett J. P. and Sridhar S., *Influence of oxygen partial pressure on synthetic coal slag infiltration into porous Al_2O_3 refractory.* Journal of the American Ceramic Society, 2012. **95**(5): p. 1764-73.
15. Scheunis L., Campforts M., Jones P. T., Blanpain B. and Malfliet A., *The influence of slag compositional changes on the chemical degradation of magnesia-chromite refractories exposed to PbO-based non-ferrous slag saturated in spinel.* Journal of the European Ceramic Society, 2015. **35**(1): p. 347-55.
16. Scheunis L., Fallah Mehrjardi A., Campforts M., Jones P. T., Blanpain B. and Jak E., *The effect of phase formation during use on the chemical corrosion of magnesia–chromite refractories in contact with a non-ferrous PbO–SiO_2 based slag.* Journal of the European Ceramic Society, 2014. **34**(6): p. 1599-610.
17. Jones P. T., Vleugels J., Volders I., Blanpain B., Van der Biest O. and Wollants P., *A study of slag-infiltrated magnesia-chromite refractories using hybrid microwave heating.* Journal of the European Ceramic Society, 2002. **22**(6): p. 903-16.
18. Jones P. T., Desmet D., Guo M., Durinck D., Verhaeghe F., Van Dyck J., Liu J., Blanpain B. and Wollants P., *Using confocal scanning laser microscopy for the in situ study of high-temperature behaviour of complex ceramic materials.* Journal of the European Ceramic Society, 2007. **27**(12): p. 3497-507.
19. Chen S., Zhao B., Jak E. and Hayes P. C., *Experimental study of phase equilibria in the PbO-MgO-SiO_2 system.* Metallurgical and Materials Transactions B-Process Metallurgy and Materials Processing Science, 2001. **32**(1): p. 11-6.
20. Lee W. E., Argent B. B. and Zhang S. W., *Complex phase equilibria in refractories design and use.* Journal of the American Ceramic Society, 2002. **85**(12): p. 2911-8.
21. Mukai K., Tao Z., Goto K., Li Z. and Takashima T., *In-situ observation of slag penetration into MgO refractory.* Scandinavian journal of metallurgy, 2002. **31**(1): p. 68-78.
22. Kim W.-Y., Pelton A. and Decterov S., *Modeling the viscosity of silicate melts containing lead oxide.* Metallurgical and Materials Transactions B, 2012. **43**(2): p. 325-36.

23. Bale C. W., Chartrand P., Degterov S. A., Eriksson G., Hack K., Ben Mahfoud R., Melancon J., Pelton A. D. and Petersen S., *FactSage thermochemical software and databases.* Calphad-Computer Coupling of Phase Diagrams and Thermochemistry, 2002. **26**(2): p. 189-228.
24. Bale C. W., Belisle E., Chartrand P., Decterov S. A., Eriksson G., Hack K., Jung I. H., Kang Y. B., Melancon J., Pelton A. D., Robelin C., and Petersen S., *FactSage thermochemical software and databases - recent developments.* Calphad-Computer Coupling of Phase Diagrams and Thermochemistry, 2009. **33**(2): p. 295-311.
25. Kuromitsu Y., Yoshida H., Takebe H. and Morinaga K., *Interaction between alumina and binary glasses.* Journal of the American Ceramic Society, 1997. **80**(6): p. 1583-7.
26. Jak E., Hayes P. C., Degterov S., Pelton A. D. and Wu P., *Thermodynamic optimization of the systems PbO-SiO_2, PbO-ZnO, ZnO-SiO_2 and PbO-ZnO-SiO_2.* Metallurgical and Materials Transactions B, 1997. **28**(6): p. 1011-8.
27. Gregurek D., Majcenovic C., Spanring A. and Kirschen M., *Forsterite bursting in magnesia chromite bricks – two case studies from lead and copper smelting furnaces.* RHI Bulletin, 2011(2): p. 49–53.